International Journal of Structural Stability and Dynamics
Vol. 16, No. 10 (2016) 1750019 (21 pages)

DOI: 10.1142/S0219455417500195

World Scientific
www.worldscientific.com

Dynamic Behavior of Damaged Bridge with Multi-Cracks Under Moving Vehicular Loads

Xinfeng Yin*§, Yang Liu*,¶, Lu Deng† and Xuan Kong‡

*School of Civil Engineering and Architecture
Changsha University of Science & Technology
Changsha 410004, Hunan, China

†College of Civil Engineering, Hunan University
Changsha 410082, Hunan, China

‡Department of Mechanical Engineering
University of Houston, Houston, TX 77004, USA
§yinxinfeng@163.com
¶liuyangbridge@163.com

Received 22 July 2015
Accepted 3 February 2016
Published

When studying the vibration of a bridge–vehicle coupled system, most researchers mainly focus on the intact or original bridge structures. Nonetheless, a large number of bridges were built long ago, and most of them have suffered serious deterioration or damage due to the increasing traffic loads, environmental effect, material aging, and inadequate maintenance. Therefore, the effect of damage of bridges, such as cracks, on the vibration of vehicle–bridge coupled system should be studied. The objective of this study is to develop a new method for considering the effect of cracks and road surface roughness on the bridge response. Two vehicle models were introduced: a single-degree-of-freedom (SDOF) vehicle model and a full-scale vehicle model with seven degrees of freedom (DOFs). Three typical bridges were investigated herein, namely, a single-span uniform beam, a three-span stepped beam, and a non-uniform three-span continuous bridge. The massless rotational spring was adopted to describe the local flexibility induced by a crack on the bridge. The coupled equations for the bridge and vehicle were established by combining the equations of motion for both the bridge and vehicles using the displacement relationship and interaction force relationship at the contact points. The numerical results show that the proposed method can rationally simulate the vibrations of the bridge with cracks under moving vehicular loads.

Keywords: Bridge; vehicle; vibration; crack; surface roughness.

1. Introduction

The bridge–vehicle interaction has attracted much attention over the past two decades owing to the significant increase of heavy vehicles running at high speeds on the highways. By modeling a moving vehicle as a moving load, moving mass, moving

sprung mass, or complicated vehicle models, the dynamic response of the vehicle was studied by many researchers.[1–6] For the bridge model in the literature, they were usually modeled as simply-supported beams[1] and multi-span continuous beams.[3,7–11] However, their studies were focused on intact bridge structures. Very few studies have considered the effect of damaged bridge structures with cracks.

As a matter of fact, a large number of bridges were built long ago, and many of them have suffered serious deterioration or damage due to the increasing traffic loads, environmental effect, material aging, and inadequate maintenance.[12,13] Few researchers have studied the effect of cracks on the vibration characteristics of damaged beams. Dimarogonas[14] studied and verified the accuracy of modeling the bridge crack with discrete spring models. Neild *et al.*[15,16] studied the nonlinear vibration characteristics of reinforced concrete damaged beams by impact excitation vibration tests. Rizzo and Scalea[17] analyzed the dynamic response of a beam with several breathing cracks to harmonic excitations. All the above studies are not related to the effect of the crack model on the vibration response of damaged beams under moving vehicles.

For the vibration of damaged bridges under moving vehicles, some studies were conducted using the simple bridge–vehicle coupled models. Lee and Ng[18] analyzed the dynamic response of a beam with a single-sided crack under a moving load. Abdel Wahab *et al.*[19] and Cheng *et al.*[20] studied the effect of crack models on the dynamic response of beams under moving loads. Mahmoud and Abou Zaid[21] studied the dynamic response of simply-supported beams with transverse cracks subjected to a moving mass. Law and Zhu[22] studied the dynamic behavior of reinforced concrete bridge structures with the damage modeled as open crack or breathing crack under the moving vehicular loads. Ariaei *et al.*[23] and Nguyen and Tran[24] studied a cracked bridge subjected to a moving vehicular load by analyzing the operational deflection time history of a vehicle–bridge system. Khoa[25] compared the open and breathing crack detections of a beam subjected to a simple moving vehicle. All the above studies are related to the simply-supported beam with simple crack model and simple vehicle model, such as the moving loads, other than the complex bridge–vehicle coupled models.

This study is mainly focused on establishing a new methodology to fully consider the effect of bridge cracks, vehicle models, and road roughness condition on the bridge behavior under moving vehicular loads. Two vehicle models were introduced: a single-degree-of-freedom (SDOF) vehicle model and a three-dimensional vehicle model with seven degrees of freedom (DOFs). The damaged bridges were modeled as three types of models, namely, a single-span uniform beam, a three-span stepped beam, and a three-span continuous non-uniform bridge deck. A model of massless rotational spring was adopted to describe the local flexibility induced by a crack in the beam. The coupled equations for the bridge and vehicle were established by combining the equations of motion for both the bridge and vehicles using the displacement relationship and interaction force relationship at the contact points. The

numerical simulations show that the proposed method can rationally simulate the vibrations of the damaged bridge under moving vehicles, and that crack plays an important role in the bridge frequencies, mode shapes, and the vibration of the vehicle–bridge coupled system.

2. Analytical Model of Vehicle–Bridge Coupled System

2.1. *Vehicular load model*

The three-dimensional analytical model for the vehicle is shown in Fig. 1. The vehicular body is assigned three DOFs, corresponding to the vertical displacement (y_t), rotation about the transverse axis (θ_t), and rotation about the longitudinal axis roll (ϕ). Each wheel/axle set is provided with two DOFs in the vertical and roll directions ($y_a^1, y_a^2, \phi_a^1, \phi_a^2$). Therefore, the total number of independent DOFs is seven.

The vertical displacements of the suspension springs can be written as:

$$U_{sy}^1 = (y_t - y_a^1) + (s_1/2)(\phi_t - \phi_a^1) + l_2\theta_t, \tag{1}$$

$$U_{sy}^2 = (y_t - y_a^1) - (s_1/2)(\phi_t - \phi_a^1) + l_2\theta_t, \tag{2}$$

$$U_{sy}^3 = (y_t - y_a^2) + (s_2/2)(\phi_t - \phi_a^2) - l_3\theta_t, \tag{3}$$

$$U_{sy}^4 = (y_t - y_a^2) + (s_2/2)(\phi_t - \phi_a^2) - l_3\theta_t, \tag{4}$$

where $U_{sy}^i (i = 1, 2, 3, 4)$ is the vertical displacements of the axles, l_2 is the distance between the front axle and the center of the vehicle, l_3 is the distance between the rear axle and the center of the vehicle, s_1 and s_2 are the distance between the right and left wheels for the front and real axles, respectively.

The vertical elastic and damping forces of the ith suspension can be written as:

$$F_{sy}^i = K_{sy}^i U_{sy}^i, \tag{5}$$

$$F_{dsy}^i = D_{sy}^i \dot{U}_{sy}^i, \quad i = 1, 2, 3, 4, \tag{6}$$

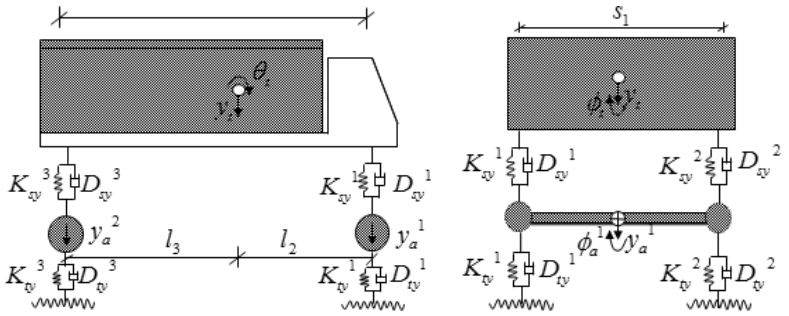

Fig. 1. Analytical model of a two-axle vehicle: (a) elevation view; (b) cross-sectional view.

where $U^i_{sy}(i = 1, 2, 3, 4)$ is the vertical displacements of the axles:

$$U^1_{tyx} = y^1_a + (s_1/2)\phi^1_a - [-r(x)^1] - y^1_{\text{b-contact}}, \tag{7}$$

$$U^2_{tyx} = y^1_a - (s_1/2)\phi^1_a - [-r(x)^2] - y^2_{\text{b-contact}}, \tag{8}$$

$$U^3_{tyx} = y^2_a + (s_2/2)\phi^2_a - [-r(x)^3] - y^3_{\text{b-contact}}, \tag{9}$$

$$U^4_{tyx} = y^2_a + (s_2/2)\phi^2_a - [-r(x)^4] - y^4_{\text{b-contact}}, \tag{10}$$

$r(x)$ denotes the vertical road surface roughness, and $y^i_{\text{b-contact}}$ the dynamic vertical deflection of the bridge at the contact position x.

The vertical interaction forces acting on the bridge surface can be written as:

$$F^i_{ty} = K^i_{ty}U^i_{ty}, \tag{11}$$

$$F^i_{dty} = D^i_{ty}\dot{U}^i_{ty}, \quad i = 1, 2, 3, 4. \tag{12}$$

The equations of motion of the full-scale vehicle can be obtained from the Lagrangian formulation, which are

$$m_t\ddot{y}_t + (F^1_{sy} + F^2_{sy} + F^3_{sy} + F^4_{sy}) + (F^1_{dsy} + F^2_{dsy} + F^3_{dsy} + F^4_{dsy}) = m_t g, \tag{13}$$

$$\begin{aligned} I_{xt}\ddot{\phi}_t &+ (s_1/2)(F^1_{sy} - F^2_{sy}) + (s_2/2)(F^3_{sy} - F^4_{sy}) + (s_1/2)(F^1_{dsy} - F^2_{dsy}) \\ &+ (s_2/2)(F^3_{dsy} - F^4_{dsy}) = 0, \end{aligned} \tag{14}$$

$$I_{zt}\ddot{\theta}_t + l_2(F^1_{sy} + F^2_{sy}) - l_3(F^3_{sy} + F^4_{sy}) + l_2(F^1_{dsy} + F^2_{dsy}) - l_3(F^3_{dsy} + F^4_{dsy}) = 0, \tag{15}$$

$$m_{a1}\ddot{y}^1_a - (F^1_{sy} + F^2_{sy}) + (F^1_{ty} + F^2_{ty}) - (F^1_{dsy} + F^2_{dsy}) + (F^1_{dty} + F^2_{dty}) = m_{a1}g, \tag{16}$$

$$\begin{aligned} I_{xa1}\ddot{\phi}^1_a &- (s_1/2)(F^1_{sy} - F^2_{sy}) + (s_1/2)(F^1_{ty} - F^2_{ty}) - (s_1/2)(F^1_{dsy} - F^2_{dsy}) \\ &+ (s_1/2)(F^1_{dty} - F^2_{dty}) = 0, \end{aligned} \tag{17}$$

$$m_{a2}\ddot{y}^2_a - (F^3_{sy} + F^4_{sy}) + (F^3_{ty} + F^4_{ty}) - (F^3_{dsy} + F^4_{dsy}) + (F^3_{dty} + F^4_{dty}) = m_{a2}g, \tag{18}$$

$$\begin{aligned} I_{xa2}\ddot{\phi}^2_a &- (s_2/2)(F^3_{sy} - F^4_{sy}) + (s_2/2)(F^3_{ty} - F^4_{ty}) - (s_2/2)(F^3_{dsy} - F^4_{dsy}) \\ &+ (s_2/2)(F^3_{dty} - F^4_{dty}) = 0, \end{aligned} \tag{19}$$

Eqs. (13)–(19) can be rewritten in a matrix form as:

$$[M_\nu]\{\ddot{y}_\nu\} + [C_\nu]\{\dot{y}_\nu\} + [K_\nu]\{y_\nu\} = \{F_G\} + \{F_{\nu-b}\}, \tag{20}$$

where $[M_\nu]$, $[C_\nu]$, $[K_\nu]$ are the mass, damping, and stiffness matrices of the vehicle, respectively; $\{y_\nu\}$ = the vector of vertical displacements of the vehicle; $\{F_G\}$ = the gravity force vector of the vehicle; and $\{F_{\nu-b}\}$ = the vector of the wheel–road contact forces acting on the vehicle.

2.2. *Vibration theory of the damaged bridge with cracks*

In the vibration study of cracked bridges, the use of massless rotational spring to describe the local flexibility induced by a crack in the beam has been verified to be accurate, leading to significant savings in the computational effort and cost of the dynamic analysis of cracked beams.[21,26,27] Therefore, in the present paper, the massless rotational spring is adopted to simulate the crack in a beam. The damaged bridge is modeled as a beam with many cracks. It is assumed that a total number of n cracks are located at sections $x_1, x_2, \ldots, x_n$, such that $0 < x_1 < x_2 \ldots < x_n < L$. The beam is divided into $n+1$ segments by the n cracks. The crack at x_i is modeled by a massless rotational spring with stiffness K_n as shown in Fig. 2.

The governing differential equation for the forced flexural vibration of the beam with variable cross-section under the moving forces can be written as:

$$\frac{\partial^2}{\partial x^2}\left[K(x)\frac{\partial^2 y_b(x,t)}{\partial x^2}\right] + \bar{m}(x)\frac{\partial^2 y_b(x,t)}{\partial t^2} + c\frac{\partial y_b(x,t)}{\partial t} = \sum_{i=1}^{4} p_i(t)\delta(x-\xi), \qquad (21)$$

where $K(x)$ is the flexural stiffness, $\bar{m}(x)$ the mass per unit length, c the damping, and $y_b(x,t)$ the vertical displacement of the beam. Using the modal superposition technique, the vertical displacement can be rewritten as $y_b(x,t) = \phi_b(x)\xi_b(t)$, where $\phi_b(x)$ is the mode shape function of the beam, and $\xi_b(t)$ is the generalized modal coordinate.

2.3. *Mode shape function of a damaged beam with cracks*

Based on Li's work,[27] the difference between a beam with a crack at the ith section and the corresponding beam without a crack is that the rotation of the cracked beam at the ith section has a jump. Therefore, the mode shape function of the cracked beam with variable cross-sections can be derived from the governing differential

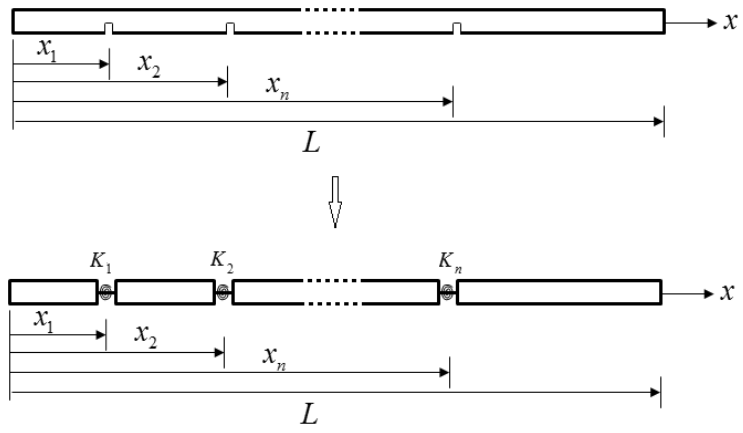

Fig. 2. The damaged beam with cracks.

equation of the intact beam with variable cross-sections. The mode shape function can be expressed as:

$$\phi_b(x) = R_1 S_1(x) + R_2 S_2(x) + R_3 S_3(x) + R_4 S_4(x), \tag{22}$$

where $S_i(x)$ and R_i $(i = 1, 2, 3, 4)$ are the linearly independent fundamental solutions and integral constants, respectively. Obviously, $S_i(x)$ are dependent on the stiffness $K(x)$ and mass per unit length $\bar{m}(x)$. Based on the results of Shifrin and Ruotolo[26] and Li,[27] the linearly independent fundamental solutions denoted by $\bar{S}_i(x)$ $(i = 1, 2, 3, 4)$ satisfy the following normalization condition at the origin of the co-ordinate system.

Using the fundamental solutions $\bar{S}_i(x)$, the mode shape function for the first interval $[0,x_1)$ can be expressed as:

$$\phi_1(x) = \phi(0)\bar{S}_1(x) + \phi'(0)\bar{S}_2(x) - \frac{M(0)}{K(0)}\bar{S}_3(x) - \frac{1}{K(0)}[Q(0) - \mu(0)M(0)]\bar{S}_4(x), \tag{23}$$

$$\mu(0) = \frac{K'(0)}{K(0)}, \tag{24}$$

where $\phi(0)$, $\phi'(0)$, $M(0)$ and $Q(0)$, respectively, denote the displacement, slope, bending moment, and shear force of the beam at $x = 0$. They are called the initial parameters in this paper, and only two of them are unknown for any kind of support configuration at $x = 0$. It is evident that $K'(0) = 0$ for a uniform beam. The displacement, bending moment, and shear force at all the boundaries of two neighboring segments are required to be continuous,

$$\phi_{i+1}(x_i) = \phi_i(x_i); M_{i+1}(x_i) = M_i(x_i); \mathcal{Q}_{i+1}(x_i) = \mathcal{Q}_i(x_i). \tag{25}$$

As introduced above, a model of massless rotational spring is adopted in this paper to describe the local flexibility induced by each crack in the non-uniform beam. If a crack is located at section $x = x_i$, the slope has a jump as,

$$\phi'_{i+1}(x_i) = \phi'_i(x_i) + \lambda_i \phi''_i(x_i), \tag{26}$$

where λ is the flexibility of the rotational spring, which is a function of the crack depth and beam height.

Considering the continuous conditions of displacement, bending moment, and shear force as well as the jump of slope at the boundary of the ith segment and the $(i + 1)$th segment, the mode shape function of the ith segment can be written as

$$\phi_{i+1}(x) = \phi_i(x) + \lambda_i \phi''_i(x_i)\bar{S}_2(x - x_i)H(x - x_i), \tag{27}$$

where $\phi_i(x)$ is the mode shape function of the ith segment (Fig. 2), $H(x)$ is the Heaviside function $x \in [x_{i-1}, x_i]$. The second term represents the jump of the slope at the boundary of the two neighboring segments. Equation (26) is a recurrence

formula for the mode shape functions. Using $\phi_1(x)$, the mode shape function of the first segment in Eq. (23), we can rewrite Eq. (27) for $i = 2, 3, \ldots, n$ as

$$\phi_{i+1}(x) = \phi_1(x) + \sum_{i=1}^{n} \lambda_i \phi''_i(x_i) \bar{S}_2(x - x_i) H(x - x_i). \tag{28}$$

2.4. *Assembling the vehicle–bridge coupled system*

Using the displacement relationship and the interaction force relationship at the contact points, the vehicle–bridge coupled system can be established by combining the equations of motion for both the bridge and vehicle, as shown below[10]:

$$\begin{bmatrix} M_b & \\ & M_v \end{bmatrix} \begin{Bmatrix} \ddot{y}_b \\ \ddot{y}_v \end{Bmatrix} + \begin{bmatrix} C_b + C_{b-b} & C_{b-v} \\ C_{v-b} & C_v \end{bmatrix} \begin{Bmatrix} \dot{y}_b \\ \dot{y}_v \end{Bmatrix} + \begin{bmatrix} K_b + K_{b-b} & K_{b-v} \\ K_{v-b} & K_v \end{bmatrix} \times \begin{Bmatrix} y_b \\ y_v \end{Bmatrix} = \begin{Bmatrix} F_{b-r} \\ F_{b-r} + F_G \end{Bmatrix}, \tag{29}$$

where C_{b-b}, C_{b-v}, C_{v-b}, K_{b-b}, K_{b-v}, K_{v-b}, F_{b-r}, and F_{b-r} are due to the wheel–bridge surface contact forces. When the vehicle moves across the bridge, the positions of the contact points as well as the values of the contact forces change, indicating that all the terms listed above are time dependent and will change as the vehicle moves across the bridge.

To simplify the bridge model and save the computation effort, the modal superposition technique is used. Using Eqs. (23) and (28), the mode shapes of the damaged beam can be obtained. The displacement vector of the damaged bridge $\{y_b\}$ in Eq. (29) can be expressed as:

$$\{y_b\} = [\,\{\Phi_1\} \quad \{\Phi_2\} \ldots \quad \{\Phi_n\}]\{\,\xi_1 \quad \xi_2 \cdots \quad \xi_n\}^T = [\Phi_b]\{\xi_b\}, \tag{30}$$

where m is the total number of modes used for the bridge; $\{\Phi_i\}$ and ξ_i are the ith mode shape of the bridge and the corresponding generalized modal coordinate, respectively. Each mode shape is normalized such that $\{\Phi_i\}^T[M_b]\{\Phi_i\} = 1$ and $\{\Phi_i\}^T[K_b]\{\Phi_i\} = \omega_i^2$.

Assuming the damping matrix $[C_b]$ in Eq. (31) to be equal to $2\omega_i\eta_i[M_b]$, where η_i is the percentage of the critical damping for the ith mode of the bridge, Eq. (29) can then be simplified into the following:

$$\begin{bmatrix} I & \\ & M_\nu \end{bmatrix} \begin{Bmatrix} \ddot{\xi}_b \\ \ddot{y}_\nu \end{Bmatrix} + \begin{bmatrix} 2\omega_i\eta_i I + \Phi_b^T C_{b-b} \Phi_b & \Phi_b^T C_{b-\nu} \\ C_{\nu-b}\Phi_b & C_\nu \end{bmatrix} \begin{Bmatrix} \dot{\xi}_b \\ \dot{y}_\nu \end{Bmatrix} + \begin{bmatrix} \omega_i^2 I + \Phi_b^T K_{b-b} \Phi_b & \Phi_b^T K_{b-\nu} \\ K_{\nu-b}\Phi_b & K_\nu \end{bmatrix} \begin{Bmatrix} \xi_b \\ y_\nu \end{Bmatrix} = \begin{Bmatrix} \Phi_b^T F_{b-r} \\ F_{\nu-r} + F_G \end{Bmatrix}. \tag{31}$$

The vehicle–bridge coupled system in Eq. (31) contains only the modal properties of the bridge and the physical parameters of the vehicles. As a result, the complexity of

Table 1. Values of $\varphi(n_0)$ for road roughness classifications.

Classifications	Ranges of $\varphi(n_0)$
Very good	from 2×10^{-6} to 8×10^{-6}
Good	from 8×10^{-6} to 32×10^{-6}
Average	from 32×10^{-6} to 128×10^{-6}
Poor	from 128×10^{-6} to 512×10^{-6}
Very poor	from 512×10^{-6} to 2048×10^{-6}

solving the vehicle–bridge coupling equations is greatly reduced. Equation (31) can be solved by the Newmark-β method in time domain.

2.5. *Bridge surface condition*

The bridge surface condition is an important factor that affects the dynamic response of both the bridge and vehicles. The bridge surface profile is usually assumed to be a zero-mean stationary Gaussian random process and can be generated through an inverse Fourier transformation based on the power spectral density (PSD) function given as follows[28–32]:

$$r(x) = \sum_{k=1}^{N} \sqrt{2\varphi(n_k)\Delta n}\cos(2\pi n_k x + \theta_k), \tag{32}$$

where θ_k is the random phase angle uniformly distributed from 0 to 2π; $\varphi()$ is the PSD function (m^3/cycle) for the bridge surface elevation; and n_k is the wave number (cycle/m). In the present study, the following PSD function has been used:

$$\varphi(n) = \varphi(n_0)\left(\frac{n}{n_0}\right)^{-2} \quad (n_1 < n < n_2), \tag{33}$$

where n is the spatial frequency (cycle/m), n_0 is the discontinuity frequency of $1/2\pi$ (cycle/m); $\varphi(n_0)$ is the roughness coefficient (m^3/cycle) whose value is chosen according to the road condition, and n_1 and n_2 are the lower and upper cut-off frequencies, respectively. The International Organization for Standardization[29] has proposed a road roughness classification index from A (very good) to H (very poor) corresponding to different values of $\varphi(n_0)$ listed in Table 1.

3. Numerical Examples

3.1. *Comparison on a uniform single-span cracked beam*

To illustrate the application of the proposed method, the normalized mid-span deflection of the beam with a moving mass is compared with the prediction by Mahmoud and Abou Zaid.[21] Figure 3 shows two beams with intact and cracked conditions under a moving mass. The parameters of the beam adopted are: length $L = 50\,\text{m}$, height $h_b = 1.0\,\text{m}$, width $B = 0.5\,\text{m}$, elastic modulus $E = 2.1 \times 10^{11}\,\text{Pa}$, and density $= 7860\,\text{kg/m}^3$. The crack at mid-span is assumed with a crack height of 0.5 m and longitudinal crack width of 0.2 mm. The moving mass is 20% of the total

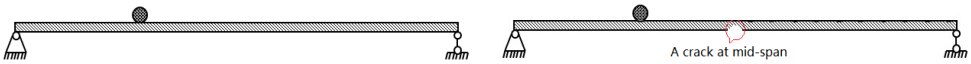

(a) (b)

Fig. 3. Two beam models subjected to a moving mass: (a) intact beam; (b) cracked beam.

mass of the beam. Comparison of the mode shapes and the normalized deflection of the intact beam and cracked beam are shown in Figs. 4 and 5.

3.1.1. *The mode shapes of the uniform cracked beam*

Based on Eq. (23) and the results of Li,[27] the solutions $S_i(x)$ for a uniform, simply-supported beam are

$$S_1(x) = e^{kx}, \quad S_2(x) = e^{-kx}, \quad S_3(x) = \sin kx, \quad S_4(x) = \cos kx, \\ k^4 = \frac{\overline{m}\omega^2}{K}. \tag{34}$$

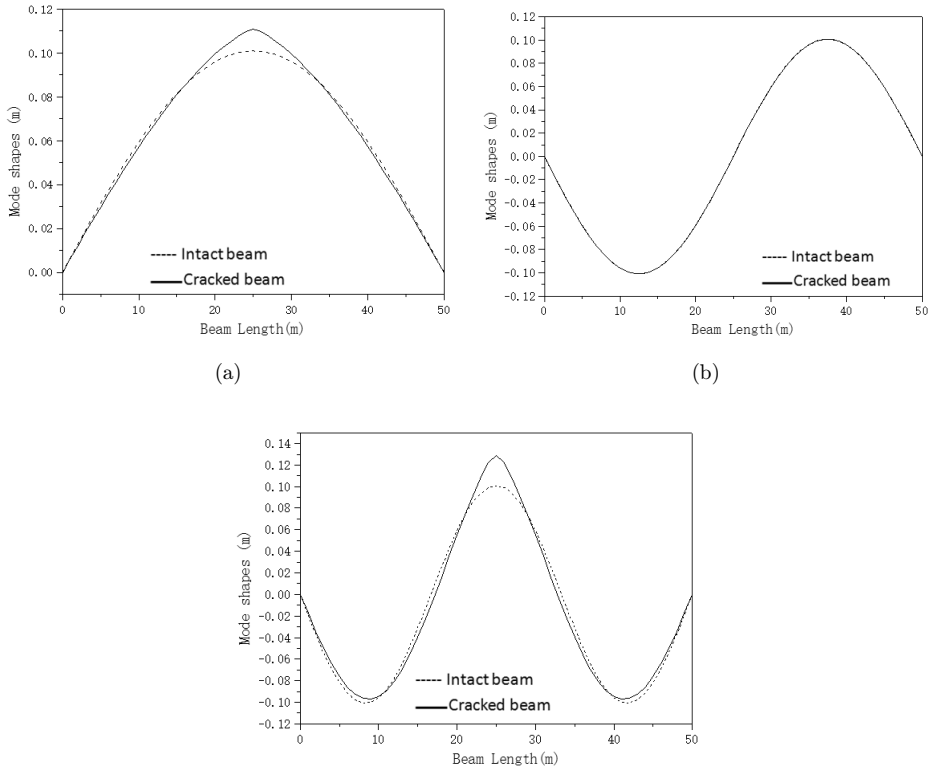

(a) (b)

(c)

Fig. 4. Mode shapes of the intact and cracked beams: (a) first mode shape; (b) second mode shape; (c) third mode shape.

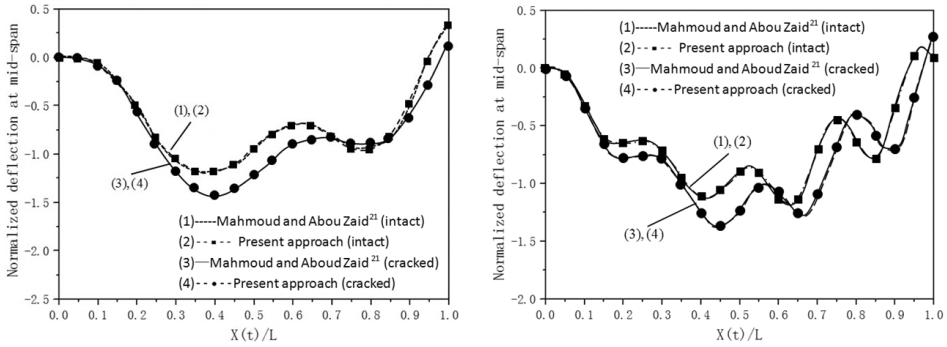

(a) (b)

Fig. 5. Comparsion of the beam deflection: (a) mass velocity $\nu = 10\,\mathrm{m/s}$; (b) mass velocity $\nu = 20\,\mathrm{m/s}$.

Using $\mathrm{S_i}(x)$ and Eq. (26), the fundamental solutions can be obtained as follows:

$$\begin{aligned}\bar{S}_1(x) &= \frac{1}{2}(\cosh(kx) + \cos(kx)), \quad \bar{S}_2(x) = \frac{1}{2k}(\sinh(kx) + \sin(kx)),\\ \bar{S}_3(x) &= \frac{1}{2k^2}(\cosh(kx) - \cos(kx)), \quad \bar{S}_4(x) = \frac{1}{2k^3}(\sinh(kx) - \sin(kx)).\end{aligned} \tag{35}$$

The mode shape function for the interval $[0,\, l/2)$ of the first segment is

$$\phi_1(x) = \phi'(0)\bar{S}_2(x) - \frac{Q(0)}{K(0)}\bar{S}_4(x), \quad x \in [0, l/2). \tag{36}$$

The mode shape function for the second segment of interval $[l/2,\, l]$ is

$$\begin{aligned}\phi_2(x) = \phi'(0)\bar{S}_2(x) - \frac{Q(0)}{K(0)}\bar{S}_4(x) + \lambda_1[X'(0)\bar{S}_2''(l/2)\\ - \frac{Q(0)}{K(0)}\bar{S}_4''(l/2)]\bar{S}_2(x - l/2), \quad x \in [l/2, l],\end{aligned} \tag{37}$$

where λ_1 is the flexibility of the rotational spring, which is a function of the crack depth and beam height; based on the study of Dimarogonas,[14] $\lambda = 5.346 h_1 f(\zeta)$, $\zeta = \frac{h_c}{h_b}$, where h_c is the height of the crack, h_b is the height of the cross-section of the beam at the crack location, and $f(\zeta) = 1.862\zeta^2 - 3.95\zeta^3 + 16.375\zeta^4 - 37.226\zeta^5 + 76.81\zeta^6 - 126\zeta^7 + 172\zeta^8 - 143.97\zeta^9 + 66.56\zeta^{10}$.

Using Eqs. (34)–(37) and the parameters of the beam, the mode shapes of the cracked beam can be obtained. Figure 4 shows a comparison of the mode shapes of the intact and cracked beam. It can be seen that because the slope of the beam at the crack location has a jump, the effect of the crack on the mode shapes is obvious.

3.1.2. *Comparison of the beam deflection*

Figure 5 shows a comparison of the beam deflection predicted by the present and existing studies. It can be seen that the present results agree excellently with those of

Mahmoud and Abou Zaid[21] for both the cracked and intact cases. In addition, the velocity of the moving mass has little effect on the present results, while the crack at the mid-span has a significant effect on the deflection of the beam under a moving mass.

3.1.3. *Effect of the number of cracks*

To study the effect of the number of cracks on the normalized deflection, three cracks with the same height and width are assumed at the locations of 1/4 span, 1/2 span, and 3/4 span. Figure 6 shows that the normalized bridge deflection increases as the number of cracks increases and the maximum normalized deflection for the beam with three cracks is 1.3 times of that for the beam with one crack.

3.2. *Three-equal-span stepped beam*

All the above studies were conducted for simply-supported beams and few have been conducted for multi-span beams. Therefore, a three-equal-span stepped beam with uniform sections at each span studied previously by Yin *et al.*[10] was adopted as the second bridge model, as shown in Fig. 7. The flexural stiffness of the central span is twice that of the side spans. Each span length is 20.0 m, and the density per unit length for all spans is assumed to be $\rho A = 1000\,\text{kg/m}$. The flexural stiffness of the

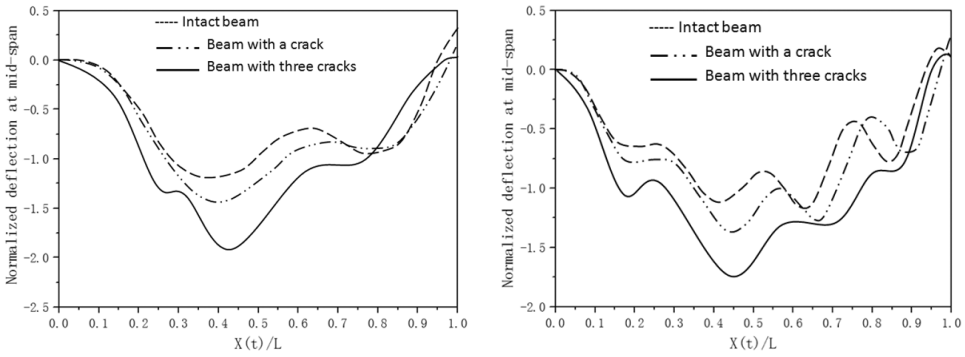

Fig. 6. Effect of the numbers of cracks on the beam deflection: (a) mass velocity $\nu = 10\,\text{m/s}$; (b) mass velocity $\nu = 20\,\text{m/s}$.

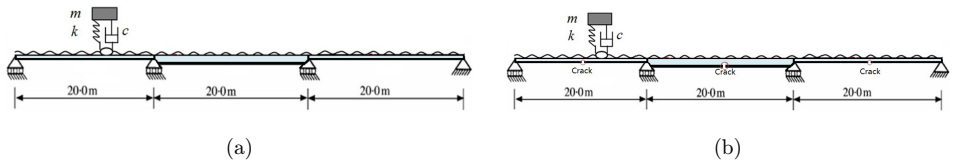

Fig. 7. Two beam models subjected to a moving vehicle model: (a) intact beam; (b) cracked beam.

side span is $EI = 1.96 \times 10^6\,\text{kN.m}^2$. The cracks at the locations of 1/4 span, 1/2 span, and 3/4 span are assumed to have a crack height of 0.5 m and width of 0.2 mm. Since the simplified moving mass in the Figs. 5 and 6 may not precisely simulate the practical vehicles on the highway bridges, a more suitable vehicle model, i.e. a SDOF vibrational system, was used to study the vibration of the cracked beam.

3.2.1. *Mode shape comparison*

Since the three equal-span stepped beam is a continuous beam, the frequencies and mode shapes of the continuous beam can be obtained as follows[30,31]:

$$\phi_{ci}(x) = \phi_i(x) + \tilde{\phi}_i(x), \tag{38}$$

where $\phi_i(x)$ are the vibration modes of a single-span beam, with a length equal to the total length of the three-span beams with the same end supports, but without the intermediate supports, and $\tilde{\phi}_i(x)$ are the augmenting cubic spline functions, which are chosen such that each $\phi_{ci}(x)$ satisfies the boundary conditions at the two ends and the zero deflection conditions at the intermediate supports. Based on Eq. (23) and Li's results,[27] the function $\phi_i(x)$ can be obtained in a way similar to Eqs. (34)–(37), and the function $\tilde{\phi}_i(x)$ can be obtained using the cubic spline expressions by satisfying all the boundary conditions. The first three natural frequencies and corresponding mode shapes calculated by the present method are shown in Table 2 and Fig. 8. As can be seen, the first frequency of the beam with three cracks is 59.7% of that of the intact beam, and the jumps occur at the locations of cracks. Therefore, the cracks can affect both the natural frequencies and mode shapes of the three-equal-span stepped cracked beam.

3.2.2. *Comparison of deflection of the cracked and intact beams*

As discussed earlier, for the simply-supported beam, the crack at the mid-span can significantly affect the deflection of the beam. In this section, the effect of cracks on the deflection of the three-equal-span stepped beam was studied. From the results shown in Fig. 9, we observe that the beam deflection increases as the number of cracks increases, and the maximum deflection of the beam with three cracks is 1.46 times that of the beam with one crack. Therefore, for the three-span stepped beam with equal spans, the cracks play an important role in the vibration of the cracked beam.

Table 2. First three natural frequencies of the cracked and intact beams.

Simulating method	First frequency (rad/s)	Second frequency (rad/s)	Third frequency (rad/s)
Intact beam	38.86	47.59	75.32
Cracked beam with a crack	37.04	47.51	70.53
Cracked beam with three cracks	23.20	43.02	66.10

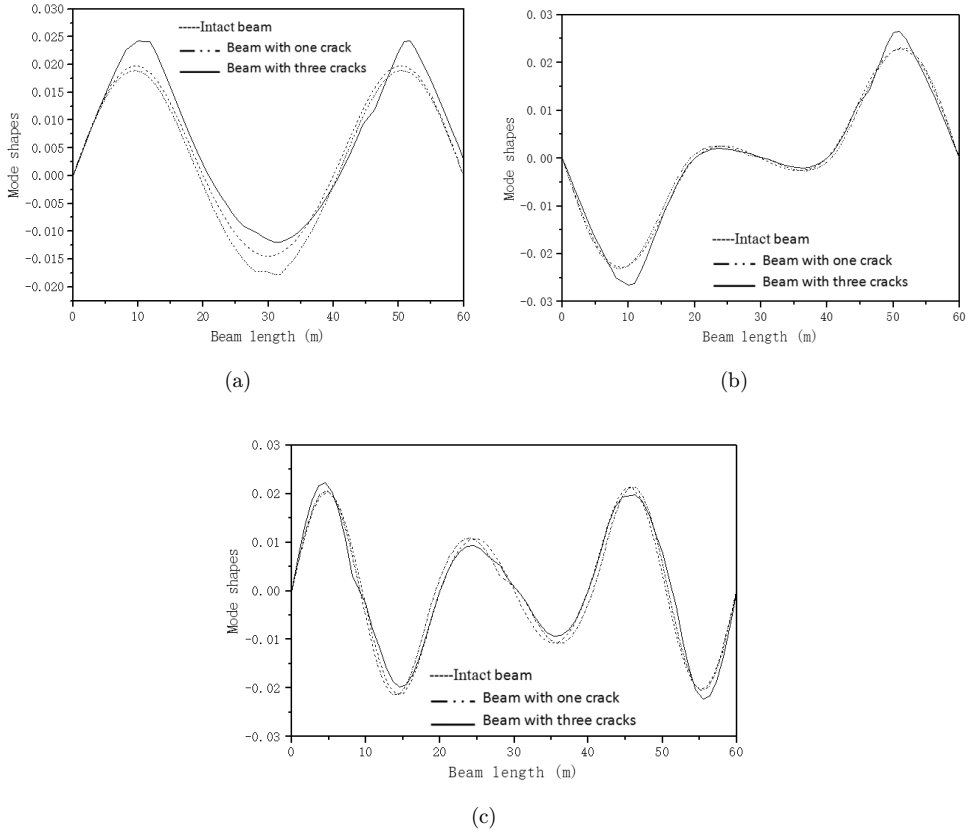

Fig. 8. Mode shapes of the intact and cracked beams: (a) first mode shape; (b) second mode shape; (c) third mode shape.

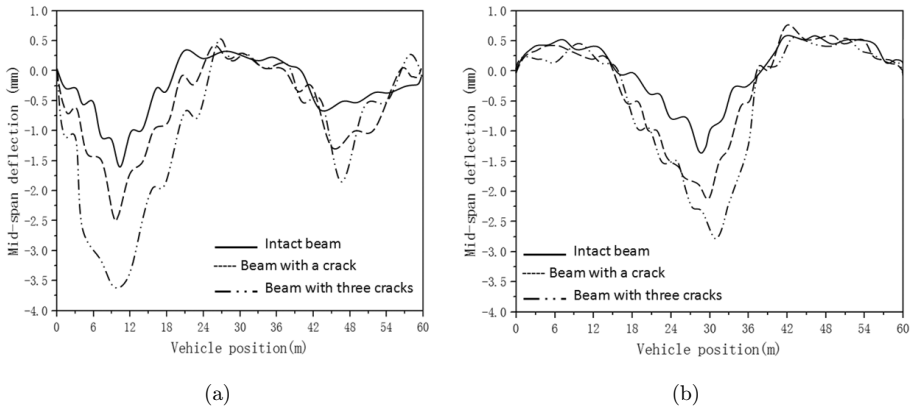

Fig. 9. Comparison of the deflection of cracked and intact beams: (a) first span; (b) central span.

3.2.3. *Effect of road surface roughness on the deflection of cracked beam*

In the previous studies by Deng and Cai,[5] Yin *et al.*,[28] and Zu,[32] the bridge surface condition was found to be an important factor that affects the dynamic response of intact bridges. Therefore, in this section, the effect of road surface roughness on the dynamic deflection is investigated. As shown in Fig. 10, the deflection of the bridge increases when the surface roughness condition changes from good to poor classifications. The maximum vertical deflection of the mid-span of the first span increases from 2.5 mm under good roughness condition to 3.25 mm under poor roughness condition. Therefore, the bridge surface condition is proven to have a large influence on the vibration of the cracked beam.

3.3. *Three-span continuous non-uniform bridge*

In the third example, the three-dimensional vehicle–bridge coupled vibrational system was adopted, which is more realistic for simulating the bridge vibration under moving vehicles. The bridge is a three-span continuous non-uniform bridge as shown in Fig. 11, and the vehicle is a full-scale vehicle model with seven DOFs as shown in Fig. 1. The modulus of elasticity of the bridge is $E = 3 \times 10^{10}\,\mathrm{N/m^2}$ and the density is $\rho = 2400\,\mathrm{kg/m^3}$. The width of the cross-section is 7.5 m, and the height of the cross-section changes from 2.0 to 4.5 m with as a function of the quadratic parabola. The cracks at the locations of 1/4 span, 1/2 span, and 3/4 span are assumed to have a crack height of 0.5 m and a width of 0.2 mm. The parameters of the full-scale vehicle are shown in Table 3.

3.3.1. *Mode shape comparison*

The difference between the mode shapes calculated for the three-span continuous non-uniform bridge model and those for the aforementioned two beam models is that

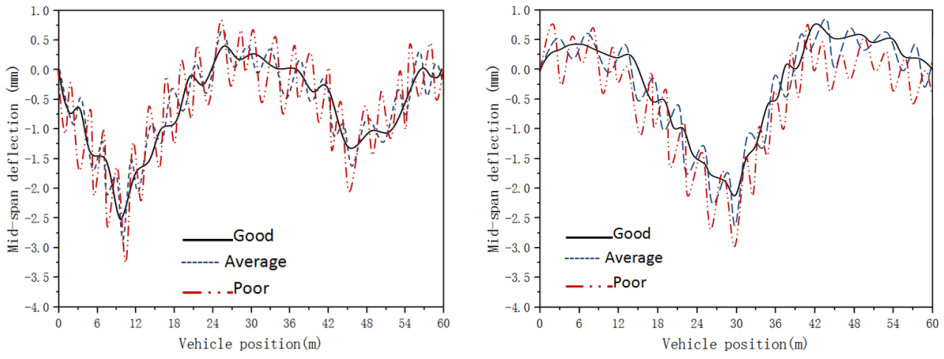

Fig. 10. Comparsion of the beam displacements under road surface roughness: (a) first span; (b) central span.

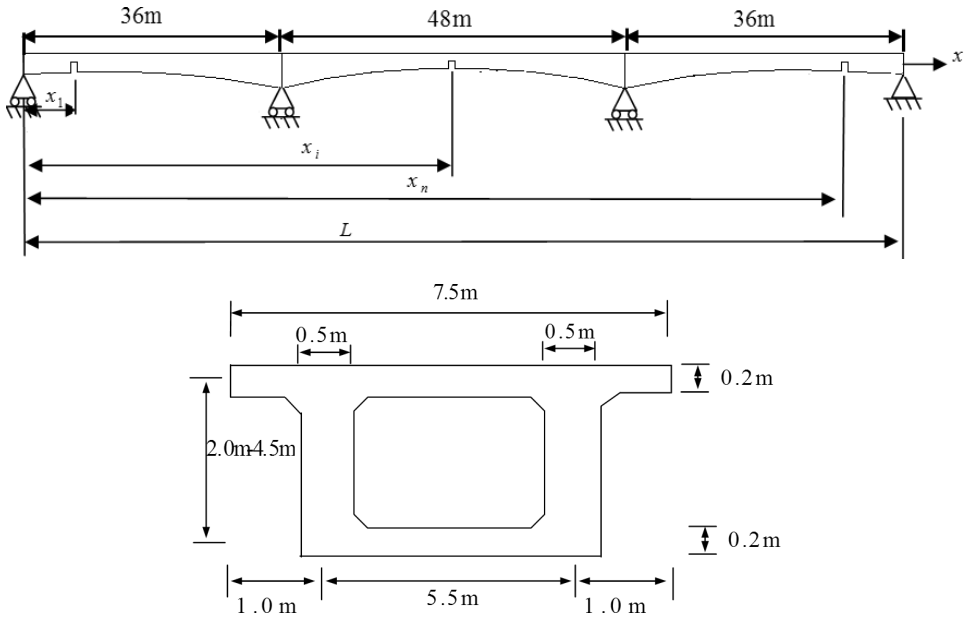

Fig. 11. Details of the three-span continuous bridge.

Table 3. The parameters of the full-scale vehicle.

Vehicle parameter	Value
Mass of truck body m_t	24808 kg
Pitching moment of inertia of truck body I_{zt}	172,160 kg.m^2
Rolling moment of inertia of truck body I_{xa1}, I_{xa2}	31,496 kg.m^2
Mass of truck front axle m_{a1}	724 kg
Mass of truck rear axle m_{a2}	800 kg
Suspension spring vertical stiffness of the first axle K^1_{sy}, K^2_{sy}	242604 (N/m)
Suspension vertical damper of the first axle D^1_{sy}, D^2_{sy}	2190 (N.s/m)
Suspension spring vertical stiffness of the second axle K^3_{sy}, K^4_{sy}	1,903,172 (N/m)
Suspension damper coefficient of the second axle D^3_{sy}, D^4_{sy}	7982 (N.s/m)
Stiffness of the tires for front axle	1,972,900 (N/m)
Stiffness of the tires for rear axle	4,735,000 (N/m)
Distance between the front and the center of the truck l_1	3.73 m
Distance between the rear axle and the center of the truck l_2	1.12 m
Distance between the right and left axles s_1	2.40 m

the flexural stiffness $K(x)$ and mass per unit length $\bar{m}(x)$ are not constant. Based on Eq. (23) and Li's results,[27] for a non-uniform beam, the flexural stiffness $K(x)$ and mass per unit length can be given as:

$$K(x) = \alpha(1+\beta x)^6, \quad \bar{m}(x) = \gamma(1+\beta x)^2, \tag{39}$$

Table 4. First three natural frequencies of the intact and cracked beams.

Simulating method	First frequency (rad/s)	Second frequency (rad/s)	Third frequency (rad/s)
Intact beam in present method	18.15	29.94	38.73
Cracked beam with a crack	17.42	29.89	36.35
Cracked beam with three cracks	16.20	28.52	34.10

where α, β, γ are the constants to be determined from the cross-sectional height distributions of the beam. The solutions $S_i(x)$ are given as:

$$S_i(x) = e^{-\lambda_i \varsigma}, \quad i = 1, 2, 3, 4, \tag{40}$$

$$\varsigma = \ln(1 + \beta x), \tag{41}$$

$$\lambda_{1,2,3,4} = -\frac{1}{2}\left(3 \pm \sqrt{1 \pm 4\left(4 + \frac{\gamma\omega^2}{\alpha}\right)}\right). \tag{42}$$

Similarly, using Eqs. (22)–(28), the function $\phi_i(x)$ of the vibration modes of a single-span beam with the same end supports but without the intermediate supports can be calculated. Considering that the cubic spline expressions $\tilde{\phi}_i(x)$ satisfy all the boundary conditions, the mode shapes and frequencies of the three-span continuous non-uniform bridge model can be obtained as shown in Table 4 and Fig. 12. Clearly, the cracks also affect the natural frequencies and mode shapes of the non-uniform three-span continuous beam.

3.3.2. *Effect of vehicle models on the deflection of cracked beam*

The time histories of the deflections at the mid-span under the three vehicle models with moving mass, simple vehicle model, and full vehicle model are plotted in Fig. 13. Clearly, deviation exists between the dynamic deflections based on the moving mass,

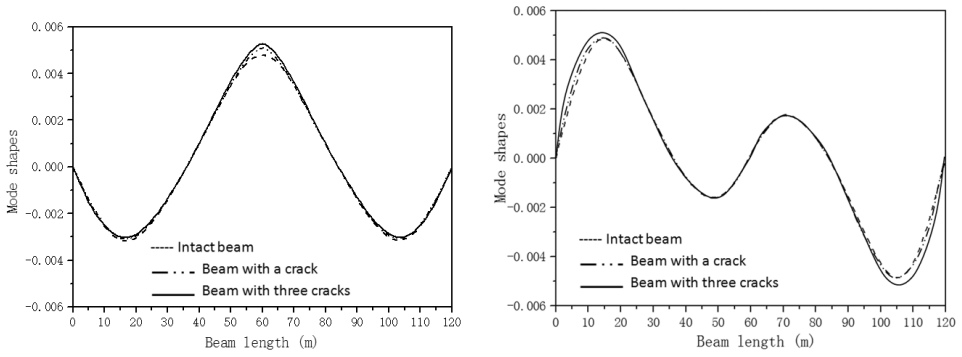

Fig. 12. Mode shapes of the intact and cracked beams: (a) first mode shape; (b) second mode shape; (c) third mode shape.

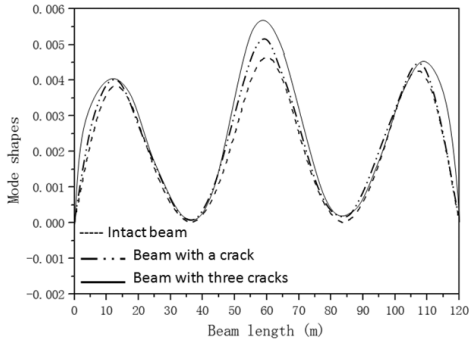

(c)

Fig. 12. (*Continued*)

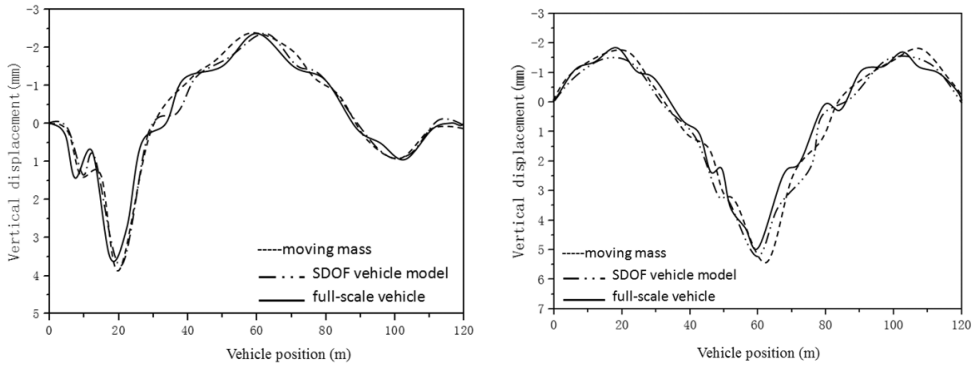

(a) (b)

Fig. 13. Effect of vehicle models on mid-span displacements: (a) first span; (b) central span.

simple vehicle model, and full vehicle model, indicating that the moving mass and simple vehicle model lose their accuracy for the dynamic deflection. Therefore, the vehicle models can affect the results of the simulation, and more realistic vehicle and bridge models should be considered in the studies.

3.3.3. *Effect of cracks on the deflection of cracked beam*

The effects of cracks on the deflection of the non-uniform three-span continuous bridge were studied with the results shown in Figs. 14 and 15. A small crack (height 0.25 m and width 0.2 mm) and a large crack (height 0.5 m and width 0.2 mm) are assumed respectively at the same position. Figure 14 shows that the beam deflection increases as damage degree increases. Figure 15 shows that the beam deflection increases as the number of cracks increases, and the maximum deflection for the first span with three cracks is 1.34 times that of the beam with one crack. Therefore, for

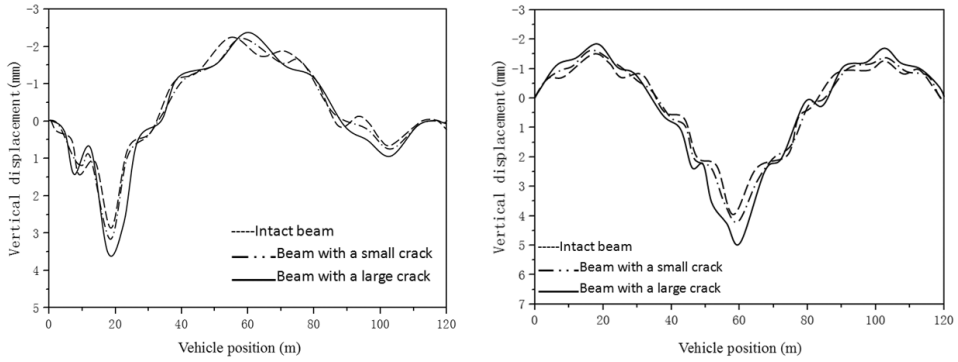

Fig. 14. Mid-span displacements of cracked and intact beams: (a) first span; (b) central span.

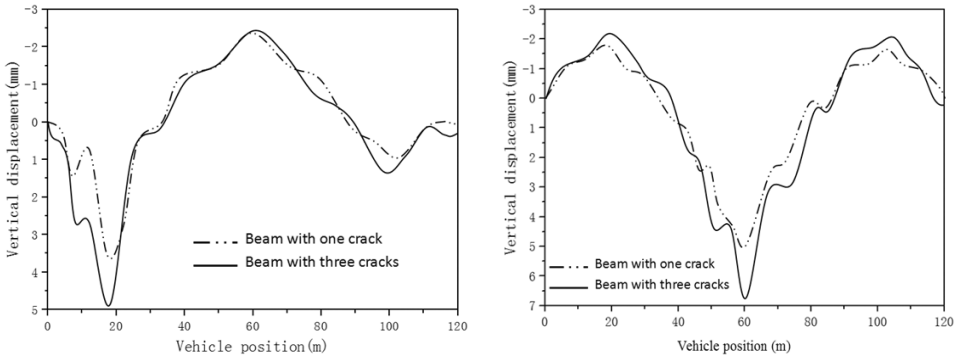

Fig. 15. Mid-span displacements of cracked and intact beams: (a) first span; (b) central span.

the non-uniform three-span continuous beam, the cracks are one of the key factors that affect the vibration of the cracked beam.

3.3.4. *Effect of road surface roughness on the deflection of cracked beam*

In this section, the effect of surface roughness on the dynamic deflection of the bridge is discussed. As shown in Fig. 16, the deflection of the bridge increases when the roughness condition changes from good to poor. The maximum vertical deflection of the mid-span of the first span increases from 3.51 mm under good roughness condition to 6.37 cm under poor roughness condition. Therefore, the surface condition has been proven to have a large influence on the vibration of damaged bridges, and regular maintenance of the bridge surface is a very effective way of reducing the vehicle-induced vibration for the bridge.

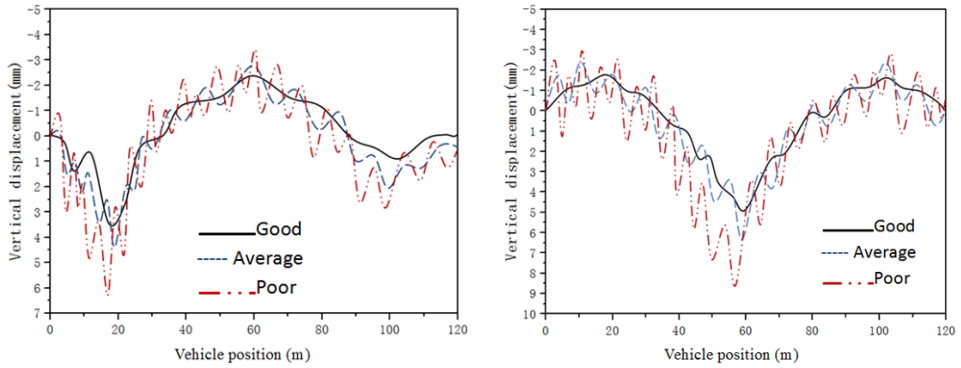

Fig. 16. Mid-span displacements under road surface roughness: (a) first span; (b) central span.

4. Conclusions

The objective of this study is develop a new approach for considering the effect of bridge cracks, vehicle models, and road surface roughness conditions on the bridge behavior under moving vehicular loads. Two vehicle models are adopted, i.e. a SDOF vehicle model and a full-scale vehicle model with seven DOFs. Three damaged bridges are considered, namely, a single-span uniform beam, a three-span stepped beam, and a three-span continuous non-uniform bridge. A massless rotational spring is adopted to describe the local flexibility induced by a crack on the bridge. The coupled equations for the bridge and vehicle system are established by combining the equations of motion for both the bridge and vehicles using the displacement relationship and interaction force relationship at the contact points. The numerical results show that: (1) the proposed method can rationally simulate the vibration of the damaged bridge under moving vehicles, and factors such as the types of vehicle and bridge models have little influence on the accuracy; (2) crack plays an important role in the bridge vibration frequencies, mode shapes, and the vibration of the vehicle–bridge coupled system; (3) the road surface condition has a large influence on the vibration of damaged bridges, and regular maintenance of the bridge surface is an effective way for reducing the vehicle-induced vibration for damaged bridges.

The successful application of the proposed method to simulate the dynamic response of a damaged bridge induced by the moving vehicles indicates that the proposed method can be applied to improving the study on the interaction between the bridge and moving vehicles. The proposed method will be further validated by field measurements from real bridges in future studies.

Acknowledgment

The authors gratefully acknowledge the financial support provided by the National Basic Research Program of China (973 Program) (Project No. 2015CB057702), the

Natural Science Foundation of China (Project No. 51108045), the Scientific Research Fund of Hunan Provincial Education Department of China (Project No. 13K051), and the Fund of Hunan Provincial Youth Talent (Project No. 2015RS4052).

References

1. L. Fryba, Response of a beam to a rolling mass in the presence of adhesion, *Acta Technica CSAV* **19**(6) (1974) 673–687.
2. T. L. Wang, D. Z. Huang and M. Shahawy, Dynamic response of multi-girder bridges, *J. Struct. Eng.* **118**(8) (1992) 2222–2238.
3. M. F. Green and D. Cebon, Dynamic interaction between heavy vehicles and highway bridges, *Comput. Struct.* **62**(2) (1997) 253–264.
4. S. R. Chen and C. S. Cai, Accident assessment of vehicles on long-span bridges in windy environments, *J. Wind Eng. Ind. Aerodyn.* **92** (2004) 991–1024.
5. L. Deng and C. S. Cai, Development of dynamic impact factor for performance evaluation of existing multi-girder concrete bridges, *Eng. Struct.* **32**(1) (2010) 21–31.
6. W. Zhang and C. S. Cai, Fatigue reliability assessment for existing bridges considering vehicle speed and road surface conditions, *J. Bridge Eng.* **17**(3) (2012) 443–453.
7. Y. B. Yang, J. D. Yau and Y. S. Wu, *Vehicle–Bridge Interaction Dynamics with Applications to High Speed Railways* (World Scientific, Singapore, 2004).
8. S. S. Law and X. Q. Zhu, Bridge dynamic responses due to road surface roughness and deceleration of vehicle, *J. Sound Vib.* **282**(3–5) (2005) 805–830.
9. S. R. Chen and J. Wu, Dynamic performance simulation of long-span bridge under combined loads of stochastic traffic and wind, *J. Bridge Eng.* **15**(3) (2010) 219–230.
10. X. F. Yin, C. S. Cai, Z. Fang and L. Deng, Bridge vibration under vehicular loads-patch contact versus point contact, *J. Struct. Stabil. Dyn.* **10**(3) (2010) 529–554.
11. Y. B. Yang, M. C. Cheng and K. C. Chang, Frequency vibration in vehicle–bridge interaction systems, *J. Struct. Stabil. Dyn.* **13**(2) (2013). doi: 10.1142/S0219455413500193.
12. C. Czaderski and M. Motavalli, 40-Year-old full-scale concrete bridge girder strengthened with pre-stressed CFRP plates anchored using gradient method, *Composites Part B: Eng.* **38** (2007) 878–886.
13. American Association of State Highway and Transportation Officials (AASHTO), LRFD bridge design specifications, Washington, DC (2004).
14. A. D. Dimarogonas, *Vibration Engineering* (West Publishers, St. Paul, Minnesota, 1996).
15. S. A. Neild, M. S. Williams and P. D. McFadden, Non-linear behavior of reinforced concrete beams under low amplitude cyclic and vibration loads, *Eng. Struct.* **24** (2002) 707–718.
16. S. A. Neild, M. S. Williams and P. D. McFadden, Nonlinear vibration characteristics of damaged concrete beams, *J. Struct. Eng.* **129**(2) (2003) 260–268.
17. P. Rizzo and F. L. Scalea, Feature extraction for defect detection in strands by guided ultrasonic waves, *Struct. Health Monit.* **5**(3) (2006) 297–308.
18. H. P. Lee and T. Y. Ng, Dynamic response of a cracked beam subject to a moving load, *Acta Mechanica.* **106** (1994) 221–230.
19. M. M. Abdel Wahab, G. De Roeck and B. Peeters, Parameterization of damage in reinforced concrete structures using model updating, *J. Sound Vib.* **228**(4) (1999) 717–730.
20. S. M. Cheng, X. J. Wu, W. Wallace and A. S. J. Swamidas, Vibrational response of a beam with a breathing crack, *J. Sound Vib.* **225**(1) (1999) 201–208.

21. M. A. Mahmoud and M. A. Abou Zaid, Dynamic response of a beam with a crack subject to a moving mass, *J. Sound Vib.* **256**(4) (2002) 591–603.
22. S. S. Law and X. Q. Zhu, Dynamic behavior of damaged concrete bridge structures under moving vehicular loads, *Eng. Struct.* **261** (2004) 279–293.
23. A. Ariaei, S. Ziaei-Rad and M. Ghayour, Vibration analysis of beams with open and breathing cracks subjected to moving masses, *J. Sound Vib.* **326** (2009) 709–724.
24. Nguyen and Tran, A multi-cracks detection technique of a beam-like structure based on the on-vehicle vibration measurement and wavelet analysis, *J Sound Vib.* **329**(21) (2010) 4455–4465.
25. V. N. Khoa, Comparisons studies of open and breathing crack detections of a beam-like bridge subjected to a moving vehicle, *Eng. Struct.* **51** (2013) 306–314.
26. E. I. Shifrin and R. Ruotolo, Natural frequencies of a beam with an arbitrary number of cracks, *J. Sound Vib.* **222** (1999) 409–423.
27. Q. S. Li, Free vibration analysis of non-uniform beam with an arbitrary number of cracks and concentrated masses, *J. Sound Vib.* **252**(3) (2002) 509–525.
28. X. F. Yin, Z. Fang and C. S. Cai, Lateral vibration of high-pier bridges under moving vehicular loads, *J. Bridge Eng.* **16**(3) (2011) 400–412.
29. ISO Mechanical Vibration-Road Surface Profiles-Reporting of Measured Data, ISO 8068: (E), Geneva (1995).
30. Y. A. Dugush and M. Eisenberger, Vibrations of non-uniform continuous beams under moving loads, *J. Sound Vib.* **254**(5) (2002) 911–926.
31. X. F. Yin, Y. Liu, S. Guo and C. S. Cai, Three-dimensional vibrations of a suspension bridge under stochastic traffic flows and road roughness, *Int. J. Struct. Stabil. Dyn.* **16** (2016). doi: 10.1142/S0219455415500388.
32. Y. Zhu, H. Xia, J. M. Goicolea and C. Xia, Bridge damage identification from moving load induced deflection based on wavelet transform and Lipschitz exponent, *Int. J. Struct. Stabil. Dyn.* (2015). doi: 10.1142/S0219455415500030.